Journal of Photochemistry and Photobiology A: Chemistry 211 (2010) 99–107

Contents lists available at ScienceDirect

Journal of Photochemistry and Photobiology A: Chemistry

journal homepage: www.elsevier.com/locate/jphotochem

Single-wall carbon nanotubes modified with organic dyes: Synthesis, characterization and potential cytotoxic effects

Gustavo M. do Nascimento[a,c,*], Rafael C. de Oliveira[a], Noriberto A. Pradie[a], Paulo R. Gessolo Lins[b], Paulo R. Worfel[b], Glaucia R. Martinez[b], Paolo Di Mascio[a], Mildred S. Dresselhaus[c,d], Paola Corio[a,*]

[a] Instituto de Química, Universidade de São Paulo, CP 26.077, CEP 05513-970, São Paulo, SP, Brazil
[b] Departamento de Bioquímica e Biologia Molecular, Universidade Federal do Paraná, Paraná, PR, Brazil
[c] Department of Electrical Engineering and Computer Science, Massachusetts Institute of Technology, ZIP 02139-4307, Cambridge, MA, USA
[d] Department of Physics, Massachusetts Institute of Technology, ZIP 02139-4307, Cambridge, MA, USA

ARTICLE INFO

Article history:
Received 27 September 2009
Received in revised form 18 January 2010
Accepted 28 January 2010
Available online 4 February 2010

Keywords:
Dyes
Carbon nanotubes
Raman
Cytotoxicity

ABSTRACT

This work deals with the covalent functionalization of single-wall carbon nanotubes (SWNTs) with phenosafranine (PS) and Nile Blue (NB) dyes. These dyes can act as photosensitizers in energy and electron transfer reactions, with a potential to be applied in photodynamic therapy. Several changes in the characteristic Raman vibrational features of the dyes suggest that a covalent modification of the nanotubes with the organic dyes occurs. Specifically, the vibrational modes assigned to the NH_2 moieties of the dyes are seen to disappear in the SWNT–dye nanocomposites, corroborating the bond formation between amine groups in the dyes and carboxyl groups in the oxidized nanotubes. The X-ray absorption (XANES) data also show, that the intense band at 398.6 eV attributed to $1s \rightarrow 2p\pi^*$ transition of the nitrogen of the aromatic PS ring, is shifted due to the bonding with the carbonic structure of the SWNTs. The cytotoxicity data of dyes-modified SWNT composites in the presence and absence of light shows that the SWNT–NB (4 μg/mL) composite presents a good photodynamic effect, namely a low toxicity in the dark, higher toxicity in the presence of light and also a reduced dye photobleaching by auto-oxidation.

1. Introduction

Single-wall carbon nanotubes (SWNTs) have unique properties, mainly due to their one-dimensional structure; such as exceptionally high tensile strength, high resilience, electronic properties ranging from metallic to semiconducting, high current carrying capacity, and high thermal conductivity [1]. The remarkable physical and chemical properties of carbon nanotubes (CNTs) have stimulated the investigation of new CNT based nanostructures, mainly those formed with polymers, metal particles and organic molecules [2,3].

Increasing interest is being focused on the rational functionalization of both single- and multiwall CNTs (MWNTs) to fabricate functionalized nanostructures with novel properties [4]. The properties of carbon nanotubes can be modified by chemical interactions, such as electrochemical and/or chemical charge-transfer processes [5,6]. Combination of both single and multiwall carbon nanotubes to organic molecules can lead to the formation of unique composites, with enhanced chemical and/or physical properties [7]. Chemical functionalization of carbon nanotubes has recently become a very important research area [8–10].

Assembly of various materials, organic and inorganic, onto the surface of CNTs has been reported. Covalent and non-covalent modifications of nanotubes properties have been explored in order to control the chemistry of CNTs. Electrochemical doping [11], electrostatic [9], covalent [12], and hydrophobic interactions have been investigated and can be used to shape their properties to specific applications. The ability to carry out controlled chemistry on the carbon nanotube surface plays an essential role in the application of these nanostructures, providing a means of purification, solubilization, biocompatibility, and diameter- or chirality-based separation [13,14].

The challenge is to find a way to reproducibly and reliably chemically alter carbon nanotubes that, like graphite, are fairly unreactive. Nowadays, the SWNTs can be chemically changed through the oxidation of their fullerene-like caps followed by different reactions with the carboxylic groups (–COOH) being formed, to make it possible to attach a large variety of chemical groups in the carbonic structure [15,16]. Functionalization of carboxylic groups with compounds that have structure like $R–NH_2$ (where the R represents different organic groups) can

* Corresponding authors at: R. Baquirivu, 197, 04404-030 São Paulo, SP, Brazil, and Av. Lineu Prestes, 748, 05513-970 São Paulo, SP, Brazil. Tel.: +55 11 56712419; fax: +55 11 56712419.
E-mail addresses: morari@yahoo.com (G.M. do Nascimento), paola@iq.usp.br (P. Corio).

1010-6030/$ – see front matter © 2010 Elsevier B.V. All rights reserved.
doi:10.1016/j.jphotochem.2010.01.019

be made by condensation reactions between amino and carboxylic groups. The reaction is mediated by condensation reagents, such as 1,3-dicyclohexylcarbodiimide (DCC) or 1-ethyl-3-(3-dimethylaminopropyl)carbodiimide (EDAC).

Fullerenes, carbon nanotubes as well as their derivatives modified with light-sensitive molecules, such as dyes, have emerged as a new interdisciplinary research field [17]. The carbonaceous materials can promote the intensification and/or prolongation of the excited states of dyes, owing to charge-transfer interactions. Photosensitizers activated by light can induce the formation of singlet oxygen or other free radicals, which can irreversibly damage the treated tissues [18,19]. It is generally accepted that singlet oxygen is the primary cytotoxic agent responsible for photobiological activity [20]. This is the background for the photodynamic therapy (PDT), which uses laser, or other light sources, combined with a light-sensitive drug (photosensitizing agent) to destroy cancer cells.

Phenazine dyes and their derivates can be induced to generate long-lived excited states which make them ideal as photosensitizers in energy and electron transfer reactions [21]. Up to now, the characterization of modified carbon nanotubes, modified with photosensitizers phenazine dyes, was scarcely investigated. The self-assembly of phenosafranine (PS dye, see Scheme 1) to acid treated multiwall carbon nanotubes (MWNTs) was investigated [22]. PS has received considerable attention due to its photoredox properties [23,24]. The authors have shown that the cationic PS dye chemisorbs in the defects along the MWNT surface. UV–vis spectroscopy reveals an electron transfer process from PS to the MWNTs π^* band. Nile Blue (NB, see Scheme 1) is a well-investigated oxazine dye and can also be used as a photosensitizing agent when attached to SWNTs in photodynamic therapy studies (PDT) [25].

The main goal of this work is the spectroscopic characterization of the nanocomposites prepared by condensation reactions between SWNTs and PS (phenosafranine) or NB (Nile Blue) dyes. In addition, the *in vitro* cytotoxic effects of these composites are also investigated.

2. Experimental

2.1. Synthesis of SWNT modified with organic dyes

2.1.1. Chemicals and materials

Organic dyes phenosafranine (PS, Aldrich, 3,7-diamino-5-phenylphenazinium chloride) and Nile Blue (NB, Merck, 5-amino-9-(diethylamino)benzo(a)phenoxazin-7-ium sulfate) were used as received. The closed-ended SWNTs carbon nanotubes (CarboLex AP-grade) are made by Arc Method. According to the producer, these carbon nanotubes have an average diameter 1.4 nm and are found in "ropes" which are typically ~20 nm in diameter or approximately 50 tubes per rope with lengths of 2–5 μm. Impurities include approximately 35 wt% residual catalysts (Ni, Y) which are usually encapsulated in carbon shells. Some amorphous carbon may also be found on the outer surfaces of the ropes. The only post-synthesis treatment of the nanotubes comes from the homogenization of the tubes directly from the chamber. Purity of CarboLex AP-grade SWNT is 70–90%.

2.1.2. Synthesis

The oxidation of SWNTs was carried out by placing 25.0 mg of SWNTs in 10.0 mL of aqueous H_2SO_4:HNO_3 (3:1) 30% solution under magnetic stirring for 6 h at room temperature (ca. 25 °C). This procedure produces SWNTs terminated with COOH groups – SWNTs(ox) [15,16]. Afterwards, the nanotubes were separated by centrifugation and washed with deionized water near to the neutral pH (ca. 6–7). The SWNTs(ox) (0.01 g) were then suspended in 50.0 mL of acetonitrile containing the dye (2.10^{-4} mol L^{-1} PS or NB). To this suspension was added 20.0 mg of 1,3-dicyclohexylcarbodiimide (DCC, Aldrich), the condensation agent (see Scheme 2). The system was stirred continually in the dark for 24 h. Then, the modified nanotubes were separated by centrifugation and washed several times with acetonitrile, ethanol and deionized water. The sample was finally separated by centrifugation and dried. This sample will be called SWNT–PS (or SWNT–NB) composite.

It should be mentioned that, for the sake of comparison, the same procedure was carried out with pristine SWNT (non-oxidized SWNT). This sample will be called SWNT + PS (or SWNT + NB). The amount of dye in the SWNT + PS and SWNT + NB samples was measured from the UV–vis data. The molar extinction coefficients were determined for PS dye (10,562 L mol^{-1} cm^{-1} at 510.0 nm) and for NB dye (76,800 L mol^{-1} cm^{-1} at 627.5 nm). From these values, it was possible to estimate that in SWNT + PS suspension the PS concentration is 6.9×10^{-5} mol L^{-1}, while for SWNT + NB suspension the NB concentration is 2.1×10^{-5} mol L^{-1}. Each suspension (50.0 mL, SWNT weight equal to 10.6 mg) was filtrated to obtain the solid material, thus, the SWNT + PS contents 9.5% of PS dye, while in SWNT + NB the percentage of NB dye is 3.5%.

2.2. Instrumentation

Raman spectra were acquired on a Renishaw Raman System 3000 equipped with a CCD detector and an Olympus microscope (BTH2) that allows a rapid accumulation of Raman spectra with a spatial resolution of about 1 μm (micro-Raman technique). The calibration of the equipment was done using a Si monocrystalline sample. The laser beam was focused on the sample by a 50× lens. Laser power was always kept below 0.7 mW at the sample in order to avoid laser-induced sample degradation. The experiments were performed under ambient conditions using a back-scattering geometry. The samples were irradiated with the 632.8 nm (1.96 eV) line of a He–Ne laser (Spectra Physics, mod. 127), and the 514.5 nm (2.41 eV) line of an Ar^+ laser (Omnichrome model 543-AP).

Fourier transform Raman (FT-Raman) spectra of solid samples were recorded using a RFS 100/S FT-Raman Bruker spectrometer with the 1064.0 nm laser line from an air-cooled diode-pumped Nd:YAG laser. Experiments were performed under room conditions

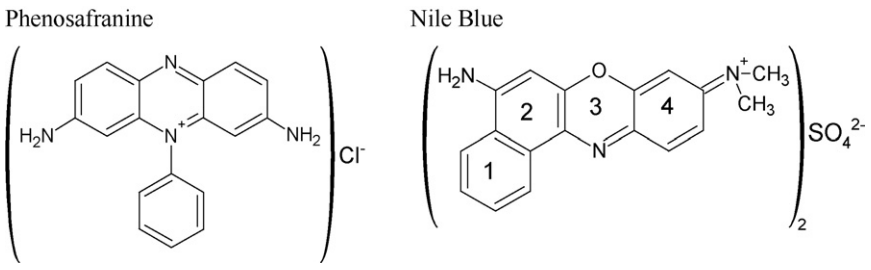

Scheme 1. Chemical structures of phenosafranine (PS) and Nile Blue (NB) organic dye molecules. The numbers from 1 to 4 were used in the assignments of the carbon rings involved in the vibrational modes shown in Table 2.

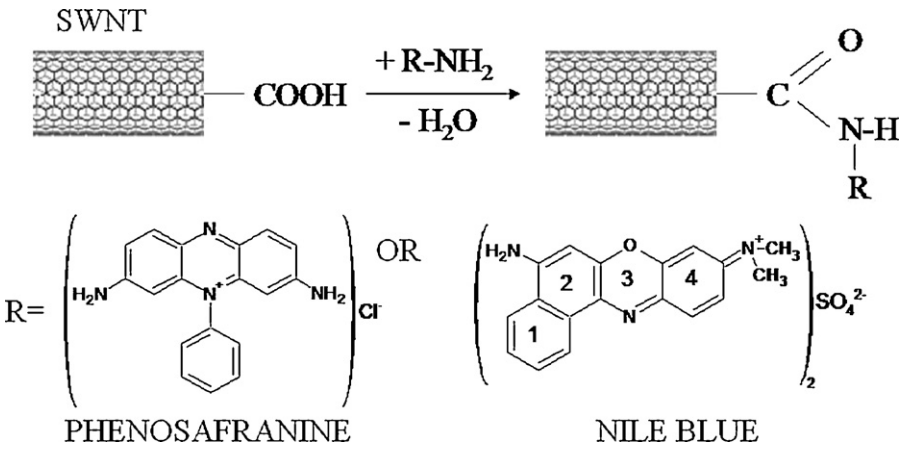

Scheme 2. Schematic representation of the chemical reactions involved in the modification of the carbon nanotubes.

with a back-scattering geometry. The laser beam with approximately 1 mm spot (the largest spot size available) was focused on the center of the aluminum disc (using the laser guided by the FT-Raman system as reference) containing the sample in the front compartment using 80.0 mW of laser power.

FTIR spectra were obtained by using a BOMEM MB-100 instrument operating with KBr optics, resolution of 4 cm^{-1}, and using DTGS detector. For collecting, the FTIR spectra, the samples were dispersed in KBr pellets.

UV–vis spectra were obtained with a Shimadzu UVPC-3101 scanning spectrophotometer using the integration sphere attached.

XANES spectra were obtained by using the facilities of the National Synchrotron Light Laboratory (LNLS), Campinas, Brazil. The spherical grating monochromator beam line (the spectral resolution $E/\Delta E$ of the spherical grating is better than 3000) has a focused beam of, roughly, a 0.5 mm^2 spot, and the spectra were recorded in the total electron yield detection mode, with the sample compartment pressure at 10^{-8} mbar. Measurements were done with the sample surface normal to the beam. All energy values in the N K-edge spectra were calibrated by using the first resonant peak in the N K-edge XANES spectrum of potassium nitrate [26,27].

2.3. Quantum chemical calculations, Raman and IR spectra

The equilibrium geometry of the PS and NB dyes, as well their respective vibrational frequencies (Raman and IR bands) were obtained with the Gaussian 03 software [28] using B3LYP density functional theory. This method uses Becke's three-parameter exchange functional (B3) [29,30], in combination with the (LYP) correlation functional [31]. All calculations were done using the 6-311++G(d,p) basis set [32,33]. The geometries of PS and NB were constrained to the C_S and C_{2V} point groups, respectively. The cutoffs on forces and step size that are used to determine optimization convergence were tightened, and the UltraFine grid option was used too, to ensure reliability of the frequencies, because low frequency vibrational modes are present. All the vibrational modes were corrected by the factor 0.9679 [34].

2.4. Cytotoxic experiments

2.4.1. Chemicals and materials

For the cytotoxic experiments dispersions of PS, NB, SWNTs, SWNTs(ox), composites of SWNT–PS and SWNT–NB (100 and 400 μg/mL) in *N*,*N*-dimethylformamide (DMF, Merck) were prepared and then further diluted with the assay medium. Solvent controls with DMF were carried out in all assays.

2.4.2. Cell line

In this work, we utilized the BHK-21 cell line (from mouse fibroblasts) acquired from Adolf Lutz institute, São Paulo, Brazil. *In vitro*, BHK-21 cells were grown with MEM and 7.5% of BPS, gentamicin at 0.125% plus 20 mmol/L of HEPES and $NaHCO_3$ at 8 mmol/L. Cells were cultivated under a 5% CO_2 atmosphere with 37 °C constant temperature. BHK-21 cells were plated (5×10^3 cells/well) 96 wells plaque and incubated at 37 °C for 24 h to achieve total adherence. After this period, cells were treated with composites and kept at 37 °C for 3 or 24 h in the dark and for 3 h under visible light irradiation (Hg lamp). For cell viability determination the

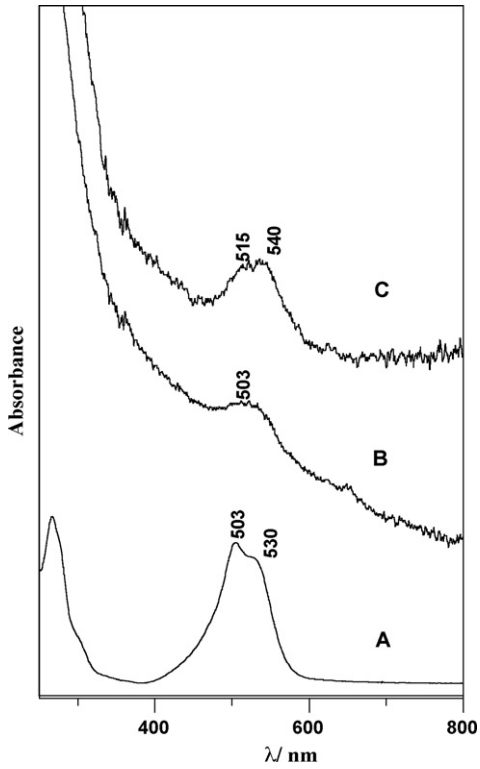

Fig. 1. UV–vis absorption spectra in acetonitrile solvent of (A) phenosafranine, (B) SWNT + phenosafranine (physical mixture) and (C) SWNT–phenosafranine composite.

MTT (3-methyl[4,5-dimethylthiazol-2yl]-2,5diphenyltetrazolium bromide) method was utilized [35].

3. Results and discussion

3.1. SWNT–PS composite

Fig. 1 shows the UV–vis spectra of plain PS (A) and a physical mixture of SWNT + PS (B) and a composite material with the SWNTs (C) in acetonitrile. In the UV–vis spectra of both, the physical mixture and the composite material, the band in the visible region at ca. 503–530 nm is observed, and this band is related to the PS dye absorption. The spectra of solutions of the composites (spectra B and C) have a high background owing to the light scattering of the suspended carbon particles. For the SWNT–PS composite is observed the higher red shift (515–540 nm) in comparison to the spectrum of plain PS dye. This red shift is due to an interaction between the PS dye and the SWNTs, probably due to the formation of covalent bonds. Indeed, Curran et al. [22] observed that the electronic absorption of PS dye shifts from 520 nm to 562 nm in the MWNT–PS composite. The authors addressed this trend to a chemisorption or bond formation, allowing a charge transfer from the PS dye to the nanotubes (an excellent electron acceptor [36]) and vice versa, thus corroborating our observation.

Resonance Raman spectra were obtained in order to monitor the changes of the vibrational states of the SWNTs. Fig. 2 displays the resonance Raman spectra at two laser lines for the pristine SWNT (2A), phenosafranine (2B), and SWNT–PS composite (2C). According to Kataura plot for pristine SWNTs [37], at E_{laser} = 2.41 eV (514.5 nm), we are in resonance with the semiconducting SWNT

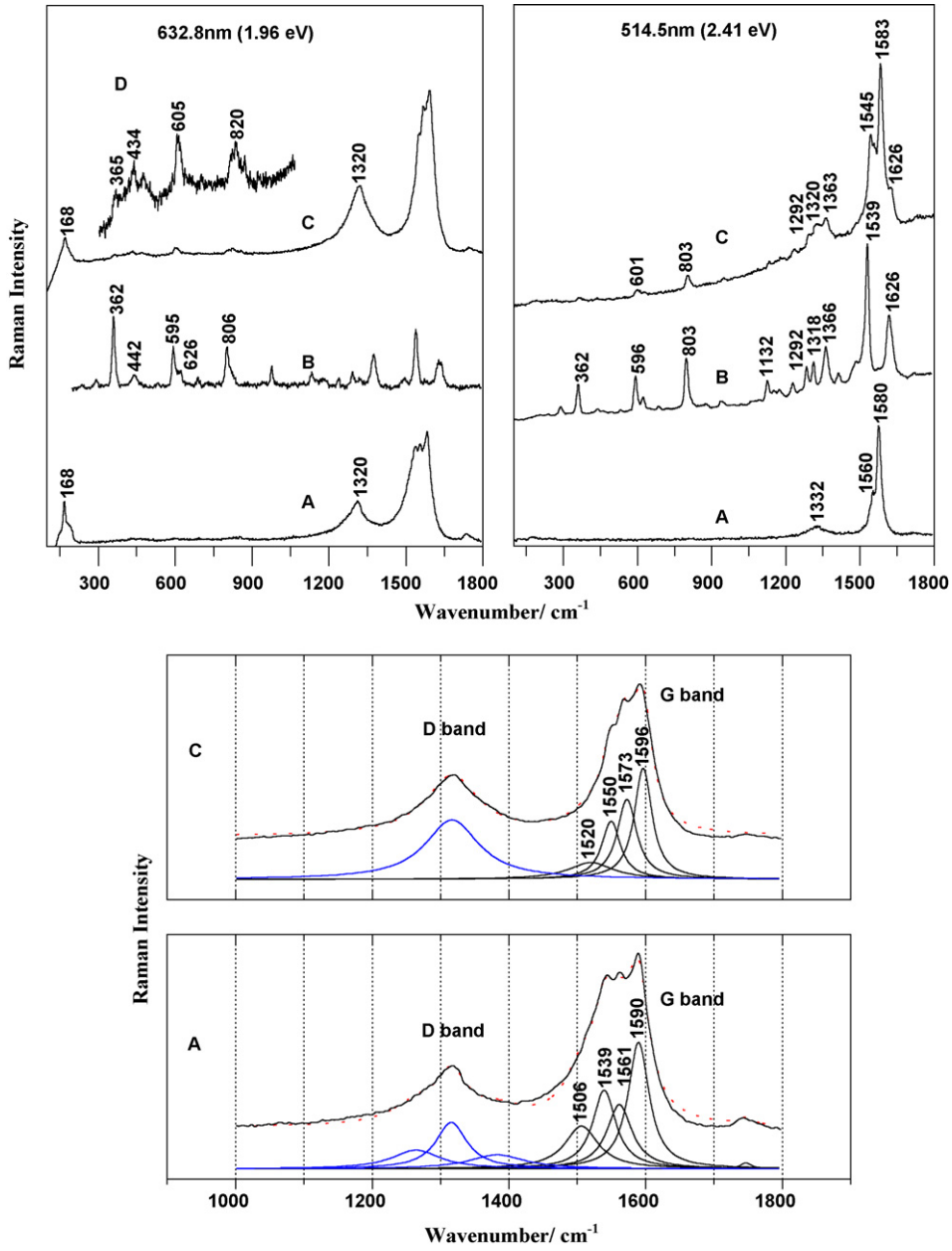

Fig. 2. Raman spectra of: pristine SWNT (A), phenosafranine (B), and SWNT–phenosafranine composite (C) at E_{laser} = 1.96 eV (632.8 nm) and E_{laser} = 2.41 eV (514.5 nm). For comparison purposes, the spectrum C is also shown, from 300 to 1100 cm^{-1}, expanded in the intensity scale (D). The deconvolution band analysis is shown for the samples A and C. The best-fit frequencies (four Lorentzian bands – black color bands – were used in the deconvolution of the G band and three Lorentzian bands – blue color bands – were used in the deconvolution of the D band) for the G band are also shown. (For interpretation of the references to color in this figure legend, the reader is referred to the web version of the article.)

Table 1
Experimental values observed in the IR spectrum and in the Raman spectra at three different laser lines (514.5, 632.8, and 1064.0 nm) for the PS dye. The equilibrium geometry of the PS dye, as well its respective vibrational frequencies (Raman and IR bands) were obtained with the Gaussian 03 software [28] using B3LYP density functional theory. The band values (with (bold) and without (italic) the numeric factor correction of 0.9679 [34]) and the assignments of the vibrational bands are given. The correlation between calculated and experimental band values was done considering the wavenumber values and relative intensities. The qualitative normal mode description for the vibrational modes was done using the visualization mode of chemcraft v.13 quantum chemistry software. The abbreviations *s*, *m*, *w*, *sh*, are related to the band intensities, and mean strong, medium, weak and shoulder. i.p. means in-plane modes. The abbreviations ν, β and γ are related to the kind of vibration modes and mean stretching, bending and torsion, respectively.

IR bands	Phenosafranine Raman bands			Calculated values B3LYP/6-311++G(d,p)		Qualitative assignment
	514.5 nm	632.8 nm	1064.0 nm			
1651 *sh*	–	–	1652 *sh*	*1671*	**1617**	$\beta(NH_2)$
1637 *m*	1639 *sh*	1636 *m*	1634 *m*	*1648*	**1595**	ν(CC), $\beta(NH_2)$
1628 *sh*	1626 *s*	–	1627 *sh*	*1569*	**1518**	$\nu(CC, CN)_{phen}$
1603 *s*	–	–	1600 *w*	*1562*	**1512**	$\nu(CC, CN)_{phen}$
–	1539 *s*	1546 *s*	1549 *s*	*1526*	**1477**	ν(CC), β(CH)
1535 *s*	1532 *sh*	–	1532 *sh*	*1515*	**1466**	ν(CC), β(CH)
–	1506 *w*	1503 *w*	1503 *s*	*1442*	**1396**	$\nu(CC, CN)_{phen}$
1485 *s*	1486 *sh*	–	1490 *sh*	*1422*	**1376**	$\nu(CC, CN)_{phen}$
1473 *sh*	–	–	–			–
–	1419 *w*	–	–			–
1387 *s*	1382 *sh*	1381 *m*	1382 *s*	*1387*	**1342**	$\nu(CC, CN)_{phen}$
–	1366 *m*	–	1362 *sh*	*1384*	**1339**	$\nu(CC, CN)_{phen}$
1323 *s*	1318 *w*	–	–	*1321*	**1278**	β(CH)
–	1292 *w*	1299 *w*	1299 *w*	*1260*	**1220**	β(CH)
1279 *w*	–	–	–			–
1244 *w*	–	1242 *w*	1245 *w*	*1215*	**1176**	β(CH)
–	1233 *w*	–	–			–
1190 *s*	1190 *sh*	–	–	*1160*	**1123**	β(CH)
1178 *sh*	1181 *w*	–	–			–
1163 *w*	1157 *w*	1158 *w*	–			–
1140 *sh*	–	1137 *w*	1141 *w*	*1159*	**1122**	β(CH)
1130 *m*	1132 *w*	–	–	*1072*	**1037**	$\gamma(NH_2)$
1072 *w*	–	–	–	*1045*	**1012**	β(CH)
–	–	–	1006 *w*	*1018*	**986**	Breathing ring
808 *w*	803 *w*	806 *m*	809 *w*	*818*	**791**	Ring torsion i.p
–	626 *w*	624 *w*	–			–
598 *sh*	596 *w*	595 *m*	599 *w*	*609*	**589**	Ring torsion i.p
443 *w*	442 *w*	446 *w*	444 *w*			–
–	362 *m*	362 *s*	365 *s*	*363*	**351**	Ring torsion i.p

tubes and at E_{laser} = 1.96 eV (632.8 nm) with the metallic ones. In addition, the laser at 514.5 nm (2.41 eV) is close to the maximum of the electronic absorption of the dye in the visible region, making it possible to study the vibrational bands of the dye owing to the resonance Raman process. In order to understand the interactions between the SWNTs and the PS, the vibrational bands of the PS dye were calculated (not found in the literature) using quantum chemical calculations. Table 1 shows the experimental and calculated values of the vibrational bands (Raman bands at different laser lines and the FTIR spectrum) of PS, and the tentative assignments that were made. The FTIR spectra for the dyes (PS and NB) used in the present work are shown in Fig. 3.

For E_{laser} = 1.96 eV, the Raman spectrum of the SWNT–PS is completely dominated by the characteristic SWNT bands, the radial-breathing mode (RBM) at 168 cm^{-1}, the D and G bands at ca. 1320 and 1590 cm^{-1}, and G′ band at 2640 cm^{-1} (not shown). Only low intensity bands are observed in the region from ca. 360 to 820 cm^{-1} and these can be related to the PS dye. By deconvolution of the G band it is possible to see more easily some changes in the G band of the SWNT and their composites. The use of four Lorentzian bands (a procedure similar to the one adopted in a previous work [37]) is enough for emulate the original G band data (see red curve in Fig. 2, spectrum A). The best fit was obtained with the bands at 1506, 1539, 1561, and 1590 cm^{-1} for the SWNT sample, while, for SWNT–PS composite, the best fit was obtained with the bands at 1520, 1550, 1573, 1596 cm^{-1} (see Fig. 2, spectrum C). Hence, a shift of the G bands is clearly observed in the spectrum of the composite in relation to the plain SWNTs. In addition, it can be seen a decrease in the relative intensities of the G bands at ca. 1520 and 1550 cm^{-1} in the spectrum of SWNT–PS composite in comparison to their counterparts in the spectrum of SWNT (bands at 1506 and 1539 cm^{-1}, respectively). These bands are assigned to the metallic SWNT tubes [38,39] and indicate that mainly metallic tubes react to the PS dye. Similarly, the G′ band also shifts from 2628 to 2640 cm^{-1}, from the Raman spectrum for the plain SWNTs (2628 cm^{-1}) to that for the composite (2640 cm^{-1}), indicating that mainly the metallic tubes react with the PS dye.

In contrast to the behavior observed at 632.8 nm, several bands related to the PS dye appear in the spectrum of the SWNT–PS composite at 514.5 nm, as a consequence of the resonance Raman

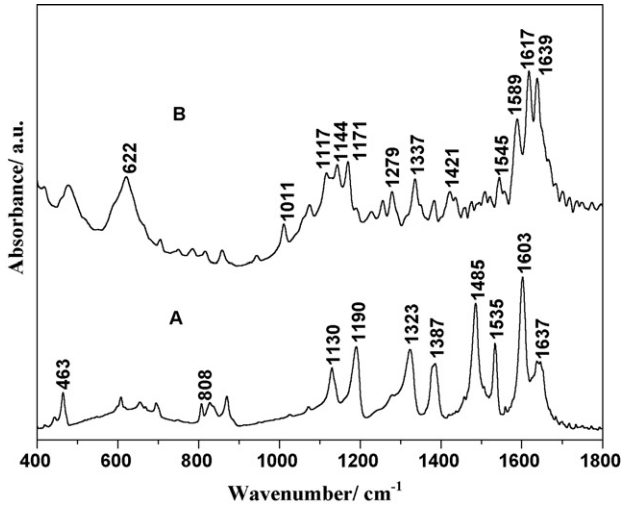

Fig. 3. FTIR spectra of solid samples dispersed in KBr pellets: phenosafranine dye (A) and Nile Blue dye (B).

behavior of the dye. The G band of the SWNTs at ca. 1580 cm^{-1} can also be observed in the spectrum. By comparing the spectra of the composite and plain dye, the main differences can be addressed: the highest PS band at 1539 cm^{-1} (assigned to the mode making the ν(CC) and β(CH) contributions, see Table 1) shifts to 1545 cm^{-1}, the band at 1132 cm^{-1} (assigned to γNH_2) also practically disappear, and finally the bands at ca. 362, 596, and 803 cm^{-1}, related to the ring torsion in plane, practically disappears in the spectrum of the SWNT–PS composite. The disappearance of the band due to the γNH_2 can be correlated with the formation of a covalent bond between the amine groups ($-NH_2$) of the dye and the carboxylic (–COOH) groups of the SWNT(ox). The shift of the highest PS band (related to the stretching of the carbons in the aromatic rings of the PS) and the decrease of the intensities of bands related with torsions can also be related to the bond of the carbon structure in the PS ring, as a consequence of the perturbing torsions of the PS ring and also the CC stretching of the rings near to the amine group.

Fig. 4 shows the fluorescence spectrum (generated by the laser at 514.5 nm) of the plain PS (A) and the composite with the SWNT (B) and finally the physical mixture of PS with SWNT (C). For the SWNT–PS composite, a shift (from ca. 700 nm to 600 nm) is observed in the fluorescence band compared to the plain PS. In addition, despite the lower intensity of the signal, the same behavior is observed for the SWNT + PS sample; probably, also, the physical adsorption of the PS on the surfaces of the carbon tube can produce the same behavior. The fluorescence shifts may be derived from an efficient energy transfer from the dye to the nanotube. A similar behavior was reported for SWNT–porphyrin hybrids [40].

X-ray absorption spectroscopy near to the Nitrogen *K*-edge (N *K* XANES) involves excitation of "core" electrons of the nitrogen atoms, and N *K* XANES is an excellent technique for distinguishing between nonequivalent nitrogen atoms [41]. Each absorption edge is related to a specific atom present in the material and, more specifically, to a quantum-mechanical transition that excites a particular atomic core-orbital electron to the free or unoccupied continuum levels (by ionization of the core orbital). In fact, the N *K* XANES spectra of "soft" matter are very complex, particularly for molecules with high electronic delocalization, since many pre-edge peaks, that can be associated to resonance and/or conjugation effects appear in such spectra [42]. Nevertheless, the N *K* XANES spectroscopy was successfully employed in the study of quinoid–benzenoid changes for aromatic and/or conjugated systems where the study of many model compounds gives assistance with the interpretation of the spectra of more complex conjugated materials [43].

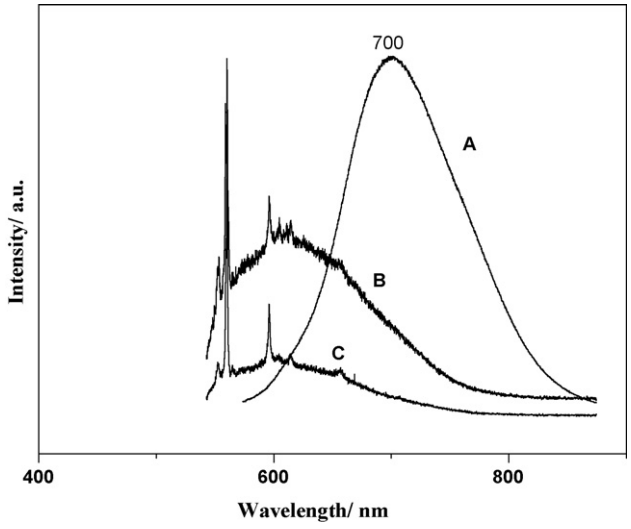

Fig. 4. Laser-induced photoluminescent of: Phenosafranine dye (A), SWNT–phenosafranine composite (B), and SWNT + phenosafranine (physical mixture) (C). E_{laser} = 2.41 eV (514.5 nm).

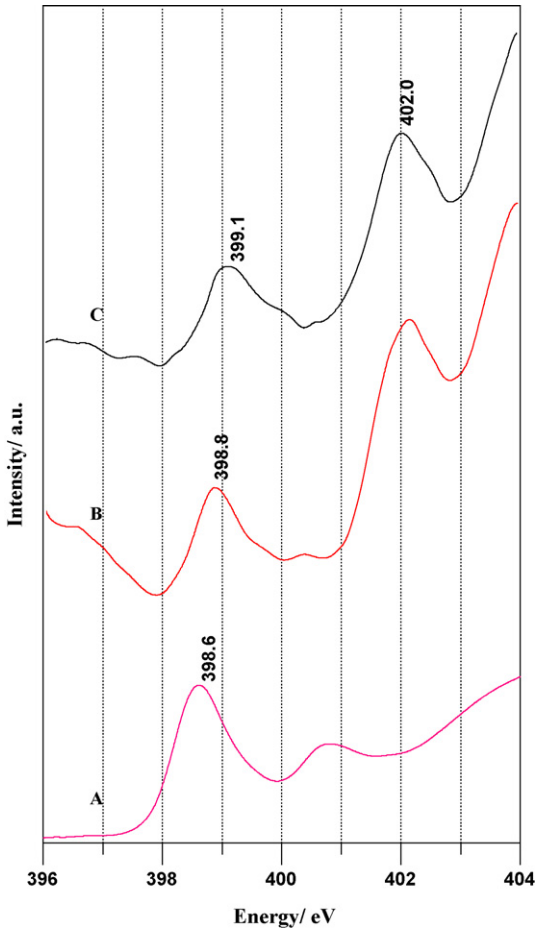

Fig. 5. N *K* XANES spectra of solid samples of: Phenosafranine dye (A), SWNT + phenosafranine (physical mixture) (B), and SWNT–phenosafranine composite (C).

Fig. 5A shows the N *K* XANES spectrum of PS dye, being the intense band at 398.6 eV that is attributed to the $1s \rightarrow \pi^*$ transition of the nitrogen in the aromatic PS ring [27,43,44]. It is clearly seen here that this peak is shifted toward higher energies in the spectra of SWNT + PS (B) and the SWNT–PS composite (C). The largest shift is observed in the spectrum of SWNT–PS composite (Fig. 5C), confirming that the electronic structure of the dye is changed due to the covalent bond with SWNTs, corroborating the Raman and UV–vis data presented above.

3.2. SWNT–NB composite

Fig. 6 shows the Raman spectra of plain SWNT, Nile Blue (NB) dye, and their SWNT–NB composite obtained with the laser excitation at 632.8 nm (1.96 eV). Here it is seen that the resonance Raman spectrum of the SWNT–NB composite is overwhelmed by bands related to the NB dye, due to the strong absorption from ca. 450 nm to 650 nm of the NB dye (not shown). It was not possible to obtain the Raman spectral information at 514.5 nm due to the strong sample fluorescence. Nevertheless, the characteristics RBM, D, G and G′ bands of the SWNT can also be observed at 1.96 eV laser line. Similarly to that observed for the SWNT–PS composite the G′ band shifts from 2628 to 2635 cm^{-1}, from the Raman spectrum for plain SWNTs to the composite, indicating that a charge-transfer reaction between metallic SWNTs and NB dye also occurred. The changes

Table 2
Experimental values observed in the IR spectrum and in the Raman spectra at two different laser lines (632.8 nm and 1064.0 nm) for the NB dye. The equilibrium geometry of the NB dye, as well its respective vibrational frequencies (Raman and IR bands) were obtained with the Gaussian 03 software [28] using B3LYP density functional theory. The band values (with (bold) and without (italic) the numeric factor correction of 0.9679 [34]) and the assignments of the vibrational bands are given. The correlation between calculated and experimental band values was done considering the wavenumber values and relative intensities. The qualitative normal mode description for the vibrational modes was done using the visualization mode of chemcraft v.13 quantum chemistry software. The abbreviations *s*, *m*, *w*, *sh*, are related to the band intensities, and mean strong, medium, weak and shoulder. The terms i.p. and o.p. mean in-plane and out-of-plane modes, respectively. The numbers 1, 2, 3, 4 are related to the Nile Blue rings, see Scheme 1. The abbreviations ν, β (s: symmetric and as: asymmetric) and γ are related to the kind of vibration modes and mean stretching, bending and torsion, respectively.

Nile Blue IR bands	Nile Blue Raman bands		Calculated values B3LYP/6-311++G(d,p)		Qualitative assignment
	632.8 nm	1064.0 nm			
1668 *sh*	–	1678 *w*	*1645*	**1593**	ν(CC)(1)
1650 *sh*	1645 *s*	1644 *s*	*1673*	**1619**	ν(CC)(4), β(NH_2)
1639 *s*	–	–	*1682*	**1628**	β(NH_2)
1617 *s*	–	1607 *w*	*1622*	**1570**	ν(CC)(1,2,4), β(NH_2)
1589 *s*	1580 *w*	1579 *w*	*1580*	**1529**	ν(CC)(1,2,3,4)
1559 *sh*	–	1549 *sh*	*1569*	**1519**	ν(CC)(1,2,3,4), β($N(CH_3)_2$)
1545 *m*	1544 *m*	1534 *m*	*1563*	**1513**	ν(CC)(1,2,3,4)
1507 *w*	–	1503 *m*	*1505*	**1456**	ν(CC)(1,2,3,4), β_{as}(CH_3)
–	1495 *m*	1494 *sh*	*1522*	**1473**	ν(CC)(4), β_{as}(CH_3)
–	–	1477 *w*	*1502*	**1453**	β_s(CH_3)
–	1442 *m*	1441 *m*	*1488*	**1441**	ν(CC)(1,2), β(CH)(1,2), β_s(CH_3)
1435 *m*	–	–	*1522*	**1473**	ν(CC)(4), β_{as}(CH_3)
1421 *m*	1424 *m*	1419 *s*	*1435*	**1389**	ν(CC)(1,2,3,4), ν(CN), β(CH)(1,2,3,4)
1385 *m*	1385 *w*	1383 *m*	*1429*	**1383**	ν(CC)(1,2,3,4), ν(CN), β(CH)(1,2,3,4)
1351 *sh*	1358 *m*	1357 *s*	*1392*	**1348**	ν(CC)(3,4)
1337 *m*	–	–	*1463*	**1416**	ν(CC)(1,2), β(CH)(1,2), β_s(CH_3)
1314 *sh*	–	1309 *m*	*1542*	**1492**	ν(CC)(4), β(CH)(4)
1289 *sh*	–	1293 *sh*			–
1279 *m*	1275 *w*	1275 *w*	*1483*	**1435**	ν(CC)(1,2,3,4), β(CH)(1,2,3,4), β_s(CH_3)
1256 *m*	1259 *w*	1252 *w*	*1500*	**1451**	ν(CC)(1,2,3,4), β_s(CH_3)
1228 *w*	–	1230 *w*	*1494*	**1446**	β_{as}(CH_3)
1191 *sh*	1195 *w*	1193 *m*	*1451*	**1405**	β_s(CH_3)
–	1185 *w*				–
1171 *s*	1170 *w*	1173 *w*	*1361*	**1318**	ν(CC)(2,3,4), β(CH)(2,3,4)
–	1154 *w*	–			–
1144 *s*	–	–	*1331*	**1289**	ν(CC)(1,2), β(CH)(1,2)
–	1138 *w*	1136 *m*	*1380*	**1334**	ν(CC)(1,4), β(CH)(1,4)
1129 *s*	–	–	*1206*	**1168**	β(CH)(1,2,3,4), ν(CC)(3)
1117 *s*	1118 *w*	1116 *w*	*1175*	**1137**	β(CH)(4)
1075 *m*	1076 *w*	1077 *m*	*1321*	**1279**	β(CH)(1,2,3,4)
1057 *sh*	1051 *w*	1046 *w*	*1291*	**1249**	β(CH)(1,2,3,4)
1011 *m*	1013 *w*	1013 *w*	*1264*	**1223**	β(CH)(1,2,3,4)
622 *s*	–	625 *w*	*779*	**754**	Ring torsion o.p.
593 *sh*	592 *s*	593 *s*	*606*	**586**	Breathing ring
–	552 *w*	555 *m*	*679*	**657**	Ring torsion i.p.

in the RBM bands from 168 and 184 (shoulder) cm^{-1} in the plain SWNTs to 160 and 174 cm^{-1} the SWNT–NB composite also indicate that a charge-transfer among the SWNTs and the NB dye occurred. The D and G bands at ca. 1320 and 1590 cm^{-1} in the spectrum of the SWNT–NB composite have practically the same relative intensity. This indicates an increase in the defects in the surface of the SWNT due to the covalent bonding of the SWNTs in the NB molecules.

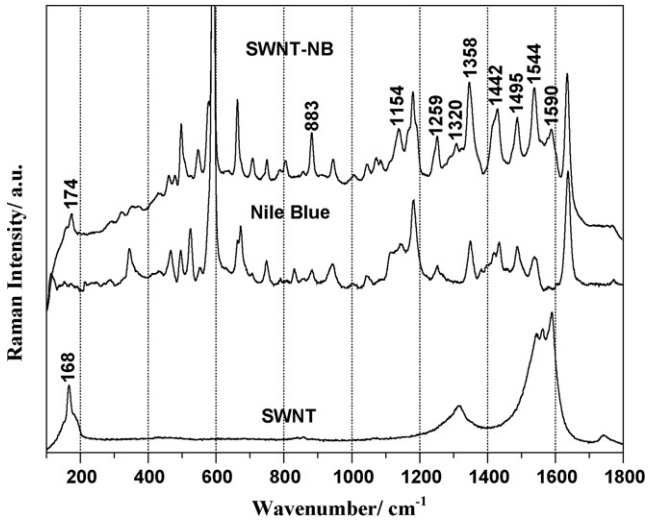

Fig. 6. Raman spectra of: pristine SWNT, Nile Blue, and SWNT–NB composite at E_{laser} = 1.96 eV (632.8 nm).

The Raman bands related to the NB dye in the Raman spectrum of the SWNT–NB composite show small frequency shifts, but the relative intensities are very different. Mainly, the bands at ca. 1544, 1495, 1442, 1358, 1259, 1154 and 883 cm^{-1}, that are related to modes formed by the stretching of the oxazine-like ring of the NB and the bending of the NH_2 and CH_3 groups (see the Table 2 for the tentative assignments). The modification of the intensities of the NB bands in addition to the changes in the characteristics of the SWNT bands strongly indicate that a charge-transfer also occurs between the NB dye and the SWNTs, likely of similar origin to that observed for the SWNT–PS composite.

3.3. Cytotoxic effects

Only phenosafranine (1 μg/mL, Fig. 7A), SWNT–NB and SWNT–PS composites (4 μg/mL, Fig. 7B) showed more cytotoxicity under light treatment. Interestingly, NB at 4 μg/mL (Fig. 7B) was 43% less toxic after irradiation, indicating a photobleaching of the dye in this condition. NB attached to SWNTs was equally toxic when incubated for 3 h under irradiation or in the dark at 1 μg/mL (Fig. 7A), as well as PS at 4 μg/mL (Fig. 7B). However, PS at 1 μg/mL (Fig. 7A) was more cytotoxic when irradiated (Fig. 7A).

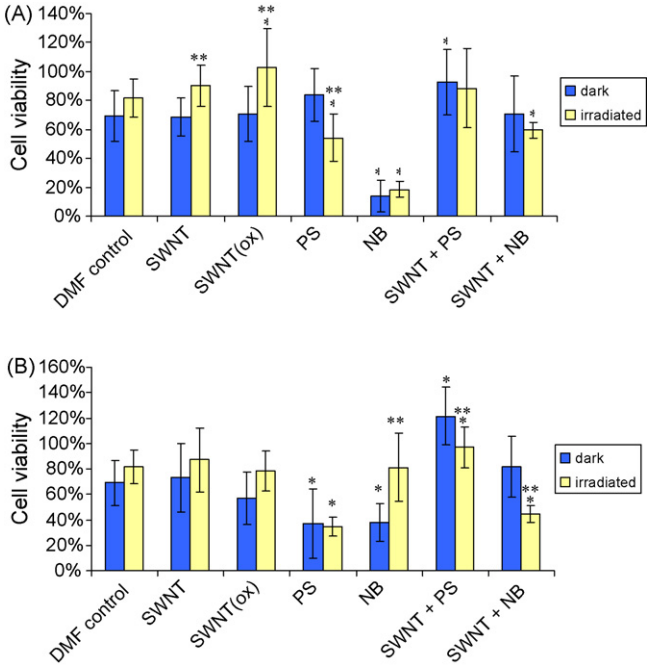

Fig. 7. Cytotoxicity in the dark and under irradiation for 3 h: plain phenosafranine (PS), plain Nile Blue (NB), and their composites at two different concentrations 1 μg/mL (A) and 4 μg/mL (B). *Statistic different compared with DMF control ($p < 0.05$) and **Statistic different compared with the correspondent incubation in the dark ($p < 0.05$).

The low toxicity observed to SWNT alone is in accordance with another study [45] that verified that cells exposed to SWNTs alone were not significantly affected. Cells exposed to concentrations of SWNTs from 0.2 to 3.2 mg mL^{-1} produced no significant toxic effects in astrocytoma cells at 24, 48, and 72 h of exposure. Another work also demonstrated that SWNT(ox) at 0.025 mg/mL has no influence in the cell viability and also in the promote apoptosis [46]. In contrast, nanotubes prepared with catalyst particles, it could generate oxidative stress and acute toxicity. Shvedova et al. [47] demonstrated a significant concentration-dependent decrease in human epidermal keratinocytes (HaCaT) viability of 11.3% (0.06 mg/mL), 24.5% (0.12 mg/mL), and 37.6% (0.24 mg/mL) after exposure to SWNT (18 h). However, incubation of HaCaT cells with a metal chelator dramatically reduced cytotoxicity of SWNTs, indicating that cytotoxicity of the SWNT was associated with iron catalytic effects.

Although DMF, even at low concentration, is not the most appropriate vehicle for biological applications, our results showed a relative low toxicity in control, which allowed to compare with SWCNT, dyes and composites treatments. New tests are been running to evaluate their properties in other cell types and different suspensions, but we show now that when dyes are linked to SWNTs their photodynamic properties change. In particular, for NB this behavior is evident, in fact Tong et al. [48] demonstrated that normal human fibroblasts showed extreme dark sensitivity to NB. Treatment with 0.1 μg/mL of NB for 1 h reduced the colony formation of normal human fibroblasts by greater than 95%. In addition, they could not detect any significant photocytotoxic effect of NB in normal human fibroblasts treated with 0.05 μg/mL and light exposure. Our results indicate that the association of NB with SWNT promotes a photocytotoxic effect without dark sensitivity.

4. Conclusions

The reactivity of single-wall carbon nanotubes with organic dyes molecules was investigated. Changes in the characteristic Raman vibrational features of the dyes suggest covalent modification of nanotubes with the organic molecules. Specifically, the vibrational modes assigned to the NH_2 moieties of the dyes are seen to disappear in the SWNT–dye nanocomposites, corroborating the bond formation between amine groups in the dyes and carboxyl groups in the SWNTs (ox). The combination of dyes and carbon nanotubes should be promising for the construction of novel hybrid materials. The photochemical properties of the dyes, including photostability and absorption and emission properties are affected by the interaction with carbon nanotubes. The cytotoxicity data for dye-modified SWNT composites in the presence and absence of light show that the SWNT–NB (4 μg/mL) composite presents a good photodynamic effect (low toxicity in the dark, higher toxicity in the presence of light and also a reduced dye photobleaching by auto-oxidation).

Acknowledgments

This work has been supported by the Conselho Nacional de Desenvolvimento Cientifico e tecnológico (CNPq) and Fundação de Amparo a Pesquisa no Estado de São Paulo (FAPESP). The authors would like to thank the National Synchrotron Light Laboratory (LNLS/Brazil) for the use of SGM beamline (XANES N *K*-edge, Proj. 2169/03). Fellowships from CNPq (G.M. do Nascimento, N.A. Pradie, P. Corio, P.G. Lins, G.R. Martinez and P. Di Mascio) are gratefully acknowledged. The authors are indebted with the LCCA (Laboratory of Advanced Scientific Computation of the University of São Paulo) for the use of its computational resources. The authors are also grateful to Rede Nacional de Pesquisas em Nanotubos de Carbono (CNPq-MCT) and Instituto do Milênio: Redoxoma, INCT de Processos Redox em Biomedicina-Redoxoma for their support. The authors from the Massachusetts Institute of Technology acknowledge the NSF for a grant (DMR 01-6915174).

References

[1] (a) M.S. Dresselhaus, G. Dresselhaus, P.C. Eklund, Science of Fullerenes and Carbon Nanotubes, Academic Press, New York, San Diego, 1996;
(b) R. Saito, G. Dresselhaus, M.S. Dresselhaus, Physical Properties of Carbon Nanotubes, Imperial Colege Press, London, 1998.
[2] D. Tasis, N. Tagmatarchis, A. Bianco, M. Prato, Chemistry of carbon nanotubes, Chem. Rev. 106 (2006) 1105–1136.
[3] G.M. Do Nascimento, P. Corio, R.W. Novickis, M.L.A. Temperini, M.S. Dresselhaus, Synthesis and characterization of single-wall-carbon-nanotube-doped emeraldine salt and base polyaniline nanocomposites, J. Polym. Sci. Part A: Polym. Chem. 43 (2005) 815–822.
[4] S.A. Curran, P.M. Ajayan, W.J. Blau, D.L. Carroll, J.N. Coleman, A.B. Dalton, A.P. Davey, A. Drury, B. McCarthy, S. Maier, A. Strevens, A composite from poly(m-phenylenevinylene-co-2,5-dioctoxy-p-phenylenevinylene) and carbon nanotubes: a novel material for molecular optoelectronics, Adv. Mater. 10 (1998) 1091–1095.
[5] G.M. Do Nascimento, T. Hou, Y.A. Kim, H. Muramatsu, T. Hayashi, M. Endo, N. Akuzawa, M.S. Dresselhaus, Double-wall carbon nanotubes doped with different Br_2 doping levels: a resonance Raman study, Nano Lett. 8 (2008) 4168–4172.
[6] S.B. Fagan, A.G. Souza, J. Mendes, P. Corio, M.S. Dresselhaus, Electronic properties of Ag^- and CrO_3-filled single-wall carbon nanotubes, Chem. Phys. Lett. 406 (2005) 54–59.
[7] S. Niyogi, M.A. Hamon, H. Hu, B. Zhao, P. Bhowmik, R. Sen, M.E. Itkis, R.C. Haddon, Chemistry of single-walled carbon nanotubes, Acc. Chem. Res. 35 (2002) 1105–1113.
[8] S. Banerjee, T. Hemraj-Benny, S.S. Wong, Routes towards separating metallic and semiconducting nanotubes, J. Nanosci. Nanotechnol. 5 (2005) 841–855.
[9] S. Banerjee, T. Hemraj-Benny, S.S. Wong, Covalent surface chemistry of single-walled carbon nanotubes, Adv. Mater. 17 (2005) 17–29.
[10] P. Corio, A. Jorio, N. Demir, M.S. Dresselhaus, Spectro-electrochemical studies of single wall carbon nanotubes films, Chem. Phys. Lett. 392 (2004) 396–402.
[11] K. Jiang, A. Eitan, L.S. Schadler, P.M. Ajayan, R.W. Siegel, Selective attachment of gold nanoparticles to nitrogen-doped carbon nanotubes, Nano Lett. 3 (2003) 275–277.
[12] S.B. Sinnott, Chemical functionalization of carbon nanotubes, J. Nanosci. Nanotechnol. 2 (2002) 113–123.
[13] V. Georgakilas, K. Kordatos, M. Prato, D.M. Guldi, M. Holzinger, M. Hirsch, Organic functionalization of carbon nanotubes, J. Am. Chem. Soc. 124 (2002) 760–761.
[14] T. Lin, V. Bajpai, T. Ji, L. Dai, Chemistry of carbon nanotubes, Aust. J. Chem. 56 (2003) 635–651.

[15] Y.-P. Sun, K. Fu, Y. Lin, W. Huang, Functionalized carbon nanotubes: properties and applications, Acc. Chem. Res. 35 (2002) 1096–1104.
[16] H. Kuzmany, A. Kukovecz, F. Simon, M. Holzweber, Ch. Kramberger, T. Pichler, Functionalization of carbon nanotubes, Synth. Met. 141 (2004) 113–122.
[17] T. Dougherty, Photosensitizers—therapy and detection of malignant-tumors, J. Photochem. Photobiol. 45 (1987) 879–889.
[18] R. Bonnett, Photosensitizers of the porphyrin and phthalocyanine series for photodynamic therapy, Chem. Soc. Rev. 24 (1995) 19–32.
[19] K.R. Gopidas, P.V. Kamat, Photophysics and photochemistry of phenosafranin dye in aqueous and acetonitrile solutions, J. Photochem. Photobiol. A: Chem. 48 (1989) 291–301.
[20] S. Wang, R. Gao, F. Zhou, M. Selke, Nanomaterials and singlet oxygen photosensitizers: potential applications in photodynamic therapy, J. Mater. Chem. 1 (2004) 487–493.
[21] M.F. Broglia, M.L. Gómez, S.G. Bertolotti, H.A. Montejano, C.M. Previtali, Photophysical properties of safranine and phenosafranine—a comparative study by laser flash photolysis and laser induced optoacoustic spectroscopy, J. Photochem. Photobiol. A: Chem. 173 (2005) 115–120.
[22] S.A. Curran, A.V. Ellis, A. Vijayaraghavan, P.M. Ajayan, Functionalization of carbon nanotubes using phenosafranin, J. Chem. Phys. 120 (2004) 4886–4889.
[23] S.S. Jayanthi, P. Ramamurthy, Excited singlet state reaction of phenosafranine with electron donors—role of the heavy-atom effect in triplet induction, J. Chem. Soc. Faraday Trans. 94 (1998) 1675–1679.
[24] K. Viswanathan, P. Natarajan, Photophysical properties of thionine and phenosafranine dyes covalently bound to macromolecules, J. Photochem. Photobiol. A: Chem. 95 (1996) 245–256.
[25] C-.W. Lin, J.R. Shulok, S.D. Kirley, L. Cincotta, J.W. Foley, Lysosomal localization and mechanism of uptake of nile blue photosensitizers in tumor-cells, Cancer Res. 51 (1991) 2710–2719.
[26] F. Rodrigues, G.M. Do Nascimento, P.S. Santos, Studies of ionic liquid solutions by soft X-ray absorption spectroscopy, J. Electron Spect. Relat. Phenom. 155 (2007) 148–154.
[27] G.M. Do Nascimento, M.L.A. Temperini, Nitrogen oxidation states elucidated by X-ray absorption nitrogen K-edge spectroscopy, Quim. Nova 29 (2006) 823–828.
[28] M.J. Frisch, G.W. Trucks, H.B. Schlegel, G.E. Scuseria, M.A. Robb, J.R. Cheeseman, J.A. Montgomery Jr., T. Vreven, K.N. Kudin, J.C. Burant, J.M. Millam, S.S. Iyengar, J. Tomasi, V. Barone, B. Mennucci, M. Cossi, G. Scalmani, N. Rega, G.A. Petersson, H. Nakatsuji, M. Hada, M. Ehara, K. Toyota, R. Fukuda, J. Hasegawa, M. Ishida, T. Nakajima, Y. Honda, O. Kitao, H. Nakai, M. Klene, X. Li, J.E. Knox, H.P. Hratchian, J.B. Cross, V. Bakken, C. Adamo, J. Jaramillo, R. Gomperts, R.E. Stratmann, O. Yazyev, A.J. Austin, R. Cammi, C. Pomelli, J.W. Ochterski, P.Y. Ayala, K. Morokuma, G.A. Voth, P. Salvador, J.J. Dannenberg, V.G. Zakrzewski, S. Dapprich, A.D. Daniels, M.C. Strain, O. Farkas, D.K. Malick, A.D. Rabuck, K. Raghavachari, J.B. Foresman, J.V. Ortiz, Q. Cui, A.G. Baboul, S. Clifford, J. Cioslowski, B.B. Stefanov, G. Liu, A. Liashenko, P. Piskorz, I. Komaromi, R.L. Martin, D.J. Fox, T. Keith, M.A. Al-Laham, C.Y. Peng, A. Nanayakkara, M. Challacombe, P.M.W. Gill, B. Johnson, W. Chen, M.W. Wong, C. Gonzalez, J.A. Pople, Gaussian 03, Revision D.01, Gaussian, Inc., Pittsburgh, PA, 2005.
[29] A.D. Becke, Density-functional thermochemistry. 1. The effect of the exchange-only gradient correction, J. Chem. Phys. 97 (1992) 9173–9177.
[30] A.D. Becke, Density-functional thermochemistry. III. The role of exact exchange, J. Chem. Phys. 98 (1993) 5648–5652.
[31] C. Lee, W. Yang, R.G. Parr, Development of the Colle–Salvetti correlation-energy formula into a functional of the electron-density, Phys. Rev. B 37 (1988) 785–789.
[32] R. Krishnan, J.S. Binckley, R. Seeger, J.A. Pople, Self-consistent molecular-orbital methods. 20. Basis set for correlated wave-functions, J. Chem. Phys. 72 (1980) 650–654.
[33] T. Clark, J. Chandrasekhar, G.W. Spitznagel, P.V.R. Schleyer, Efficient diffuse function-augmented basis-sets for anion calculations. 3. The 3-21+G basis set for 1st-row elements, LI-F, J. Comput. Chem. 4 (1983) 294–301.
[34] M.P. Andersson, P. Uvdal, New scale factors for harmonic vibrational frequencies using the B3LYP density functional method with the triple-xi basis set 6-311+G(d,p), J. Phys. Chem. A 109 (2005) 2937–2941.
[35] T.P. Reilly, F.H. Bellevue, P.M. Woster, C.K. Svensson, Comparison of the in vitro cytotoxicity of hydroxylamine metabolites of sulfamethoxazole and dapsone, Biochem. Pharm. 55 (1998) 803–810.
[36] A.M. Rao, P.C. Eklund, S. Bandow, A. Thess, R.E. Smalley, Evidence for charge transfer in doped carbon nanotube bundles from Raman scattering, Nature 388 (1997) 257–259.
[37] H. Kataura, Y. Kumazawa, Y. Maniwa, I. Umezu, S. Suzuki, Y. Ohtsuka, Y. Achiba, Optical properties of single-wall carbon nanotubes, Synth. Met. 103 (1999) 2555–2558.
[38] M.A. Pimenta, A. Marucci, S.A. Empedocles, M.G. Bawendi, E.B. Hanlon, A.M. Rao, P.C. Eklund, R.E. Smalley, G. Dresselhaus, M.S. Dresselhaus, Raman modes of metallic carbon nanotubes, Phys. Rev. B 58 (1998) R16016–16019.
[39] S.D.M. Brown, P. Corio, A. Marucci, M.S. Dresselhaus, M.A. Pimenta, K. Kneipp, Second-order resonant Raman spectra of single-walled carbon nanotubes, Phys. Rev. B 61 (2000) R5137–R5140.
[40] H. Murakami, T. Nomura, N. Nakashima, Noncovalent porphyrin-functionalized single-walled carbon nanotubes in solution and the formation of porphyrin-nanotube nanocomposites, Chem. Phys. Lett. 378 (2003) 481–485.
[41] P.J. Durham, Theory of XANES, in: D.C. Koningsberger, R. Prins (Eds.), X-ray Absorption, John Wiley & Sons, New York, 1988, pp. 53–86.
[42] (a) C. Hennig, K.H. Hallmeier, A. Bach, S. Bender, R. Franke, J. Hormes, R. Szargan, Influence of substituents on the N K X-ray absorption near-edge structure of pyrrole derivatives, Spectrochim. Acta A 52 (1996) 1079–1083;
(b) C. Hennig, K.H. Hallmeier, R. Szargan, XANES investigation of chemical states of nitrogen in polyaniline, Synth. Met. 92 (1998) 161–166.
[43] J.T. Francis, A.P. Hitchcock, Inner-shell spectroscopy of para-benzoquinone, hydroquinone, and phenol—distinguishing quinoid and benzenoid structures, J. Phys. Chem. 96 (1992) 6598–6610.
[44] G.M. Do Nascimento, V.R.L. Constantino, R. Landers, M.L.A. Temperini, Aniline polymerization into montmorillonite clay: a spectroscopic investigation of the intercalated conducting polymer, Macromolecules 37 (2004) 9373–9385.
[45] L. Dong, K.L. Joseph, C.M. Witkowski, M.M. Craig, Cytotoxicity of single-walled carbon nanotubes suspended in various surfactants, Nanotechnology 19 (2008) 255702.
[46] N.W.S. Kam, H. Dai, Functionalization of carbon nanotubes via cleavable disulfide bonds for efficient intracellular delivery of siRNA and potent gene silencing, J. Am. Chem. Soc. 127 (2005) 6021–6026.
[47] A.A. Shvedova, V. Castranova, E.R. Kisin, D. Schwegler-Berry, A.R. Murray, V.Z. Gandelsman, A. Maynard, P.J. Baron, Exposure to carbon nanotube material: assessment of nanotube cytotoxicity using human keratinocyte cells, Toxicol. Environ. Health Part A 66 (2003) 1909–1926.
[48] Z. Tong, G. Singh, A. Rainbow, Extreme dark cytotoxicity of Nile Blue A in normal human fibroblasts, J. Photochem. Photobiol. 74 (2001) 707–711.